Collectivity of ^{196}Po at low spin

T. Grahn,[1,*] A. Dewald,[2] P. T. Greenlees,[3] U. Jakobsson,[3] J. Jolie,[2] P. Jones,[3] R. Julin,[3] S. Juutinen,[3] S. Ketelhut,[3] T. Kröll,[4] R. Krücken,[4] M. Leino,[3] P. Maierbeck,[4] B. Melon,[2] M. Nyman,[3] R. D. Page,[1] P. Peura,[3] Th. Pissulla,[2] P. Rahkila,[3] J. Sarén,[3] C. Scholey,[3] J. Sorri,[3] J. Uusitalo,[3] M. Bender,[5,6] and P.-H. Heenen[7]

[1]*Department of Physics, Oliver Lodge Laboratory, University of Liverpool, Liverpool L69 7ZE, United Kingdom*

[2]*Institut für Kernphysik, Universität zu Köln, Zülpicher Str. 77, D-50937 Köln, Germany*

[3]*Department of Physics, University of Jyväskylä, P. O. Box 35, FI-40014 Jyväskylä, Finland*

[4]*Physik-Department E12, TU München, D-85748 Garching, Germany*

[5]*Université Bordeaux, Centre d'Etudes Nucléaires de Bordeaux Gradignan, UMR5797, F-33175 Gradignan, France*

[6]*CNRS/IN2P3, Centre d'Etudes Nucléaires de Bordeaux Gradignan, UMR5797, F-33175 Gradignan, France*

[7]*Service de Physique Nucléaire Théorique, Université Libre de Bruxelles, C.P. 229, B-1050 Bruxelles, Belgium*

(Received 27 May 2009; published 31 July 2009)

Absolute electromagnetic transition probabilities in ^{196}Po have been measured using the recoil distance Doppler-shift technique. The lifetimes of the three lowest yrast states in ^{196}Po were extracted from singles γ-ray spectra by using the recoil-decay tagging method. In addition, configuration mixing calculations of angular momentum projected mean-field states have been carried out for ^{196}Po. The present study sheds light on the onset of collectivity and mixing of competing structures in neutron-deficient Po nuclei.

DOI: 10.1103/PhysRevC.80.014323 PACS number(s): 21.10.Ky, 21.10.Tg, 23.20.−g, 27.80.+w

I. INTRODUCTION

Collective excitations based on coexisting minima in a potential energy surface have been widely explored, particularly in the vicinity of $Z = 82$ nuclei around the neutron midshell at $N = 104$. The mechanism giving rise to the deformed minima has been extensively studied (see, e.g., [1,2]), and recently complementary theoretical and experimental approaches have been used to shed more light on the underlying nuclear structure in this region [3,4].

Polonium nuclei, having just two protons outside the $Z = 82$ shell closure, have been shown to exhibit a wide range of structural changes as a function of neutron number. The low-energy structure of ^{210}Po is explained with the two valence protons occupying the nuclear shell model orbitals. When moving away from the $N = 126$ shell closure toward the neutron midshell the number of valence particles becomes large and the shell model description becomes less successful. The two valence protons interact with neutrons in the open $N = 126$ shell and consequently, when approaching the neutron midshell, the onset of quadrupole collectivity is expected.

In ^{196,198,200,202}Po intruding 0^+ states, similar to those observed in neutron deficient Pb nuclei [5], have been observed in α- and β-decay studies and associated with a $\pi(4p\text{-}2h)$ configuration [6] and an oblate minimum [7]. Accordingly, observed yrast states in the light even-mass $^{192-196}$Po nuclei are presumed to form oblate bands [2]. The collective intruder character of low-lying yrast states was recently verified by a lifetime measurement in ^{194}Po [8]. Furthermore, in Po nuclei with $A \leqslant 191$, the prolate configuration comes down in energy [9,10], reaching the ground state at ^{188}Po [11].

In Po isotopes with $A > 194$ the deformed intruder structures are expected to lie higher in energy and mixing of near-spherical and deformed states is expected to occur at low spin. Within a simple mixing model, intruder contributions of $\sim$10% in the ground state and $\sim$70% in the 2^+ yrast state in ^{196}Po have been deduced [6]. Moreover, recent experimental and theoretical investigations have revealed a predominant intruder character of the ground state of ^{194}Po [4].

Rather than associating the collectivity in the neutron deficient Po nuclei to intruder configurations and consequently shape coexistence, an alternative approach was taken in Ref. [12]. Due to the relatively small number of valence particles, observed nearly equal level spacings and a near degeneracy of the 4_1^+ and 2_2^+ states, the low-spin structure of ^{196}Po was interpreted using a vibrational model. A level scheme of ^{196}Po is shown in Fig. 1, where members of the suggested two and three phonon multiplets can indeed be identified. However, this picture cannot explain the occurrence of the low-lying 0^+ state at 558 keV [6].

While a variety of theoretical studies of the shape coexistence in Pb nuclei is available, the theoretical information concerning the neutron-deficient Po nuclei is still somewhat scarce. The first theoretical evidence of the shape transitions in Po nuclei, by using the Nilsson-Strutinsky method, was found in Ref. [7]. A different approach was taken in Ref. [13], where the configuration mixing between spherical and intruder structures was studied in various theoretical frameworks. Both of these studies predict the oblate structure gradually to drop down in energy in Po isotopes with $A < 200$, finally reaching the ground state at ^{192}Po.

More information about the nature of collectivity and configuration mixing can be obtained from electromagnetic transition probabilities between relevant states. Striking examples of this are ^{186,188}Pb, where the transition from the first excited (mixed) 2^+ state to the spherical ground state is noncollective due to the change in structure between

*tuomas.grahn@liverpool.ac.uk

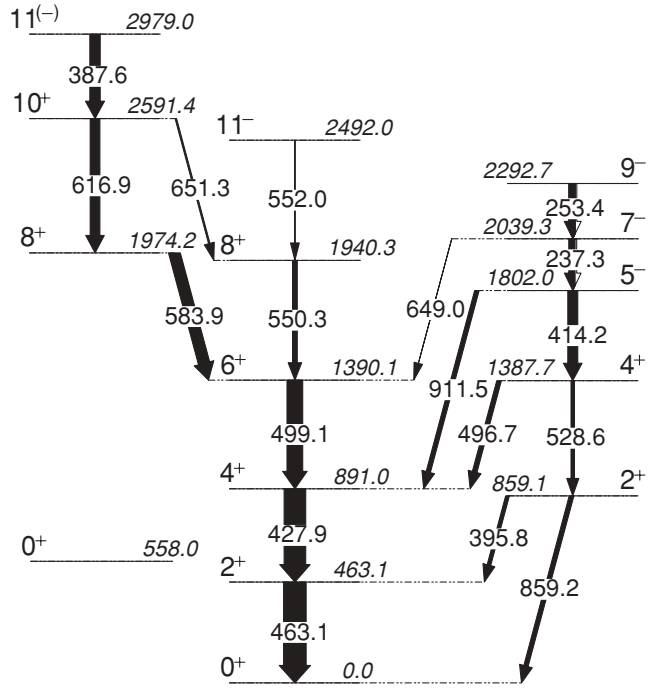

FIG. 1. A partial level scheme of ^{196}Po. Level and transition energies are given in keV and the widths of the arrows are proportional to the γ-ray intensities. This figure has been reproduced from the data taken from Ref. [12]. The 2492 keV 11^- isomeric state is taken from Ref. [14] and the excited 0^+ state from Ref. [6].

the two states [8]. Therefore, in the present work, a recoil distance Doppler-shift (RDDS) lifetime measurement similar to the earlier one for ^{194}Po [8] has been carried out for the low-lying yrast states ^{196}Po. In addition, configuration mixing calculations of angular momentum projected mean-field states have been carried out for ^{196}Po. Such calculations were earlier used in a successful description of collective properties of ^{186,188}Pb and ^{194}Po nuclei [4].

II. EXPERIMENTAL DETAILS AND RESULTS

Excited states of ^{196}Po were produced using a heavy ion induced fusion-evaporation reaction at the Accelerator Laboratory of the University of Jyväskylä. The reaction ^{113}Cd(^{86}Kr,$3n$)^{196}Po at a beam energy of 382 MeV was employed, providing an initial recoil velocity of $v/c = 3.5\%$. In the present RDDS measurement, the Köln plunger device was combined with the JUROGAM Ge-detector array and the gas-filled recoil separator RITU [15]. A stretched 1 mg/cm^2 ^{113}Cd target with a 1 mg/cm^2 Ta support facing the beam was used. A standard stopper foil of the plunger device was replaced by a 1 mg/cm^2 Mg foil in order to allow fusion-evaporation residues to recoil into RITU. Prompt γ rays were detected with the JUROGAM Ge-detector array consisting of 43 Eurogam Phase I type Compton-suppressed Ge detectors [16].

Fusion-evaporation residues were separated in-flight from the beam and other reaction products according to their magnetic rigidity by RITU and detected at the focal plane by the GREAT spectrometer [17]. The selection of recoils was made combining the timing and energy loss information of the multiwire proportional counter at the entrance of GREAT with the timing information of the double-sided silicon strip detectors (DSSDs). The α decays originating from the 0^+ ground state of ^{196}Po ($E_\alpha = 6520$ keV, $t_{1/2} = 5.73$ s) were detected with the DSSDs and spatially and temporally correlated with the detected recoils. Hence, prompt γ rays were assigned to ^{196}Po according to the principles of the recoil-decay tagging (RDT) method [18]. The data were collected using the triggerless Total Data Readout data acquisition system [19].

The data were recorded with 13 different target-to-degrader distances, ranging from 20 μm to 6 mm. RDT singles γ-ray spectra for ^{196}Po were reconstructed offline using the GRAIN software package [20]. For the final RDDS analysis only 15 of the JUROGAM Ge detectors, five at an angle of 158° and ten at an angle of 134° with respect to the beam direction, could be used due to their suitable angular position. The separation of the fully Doppler-shifted and degraded components in the final γ-ray spectra was typically of the order of 3 keV.

Lifetimes of the $2^+, 4^+$, and 6^+ yrast states in ^{196}Po were extracted using the differential decay curve method (DDCM) [21]. The intensities of both components of the γ-ray transitions under study were normalized by the sum of the fully-shifted (I_s) and degraded components (I_d) and decay curves $I_s/(I_d + I_s)$ were constructed. The known isomeric 11^- state at 2492 keV has a half-life of $t_{1/2} = 850$ ns [14] and therefore has no influence on the present prompt lifetime measurement. Samples of spectra and typical two component fits are illustrated in Fig. 2.

Both the 2^+ and the 4^+ states were populated up to 92% and the 6^+ state up to 43% by the direct feeding transitions observed in the present work. In a singles RDDS measurement, the influence of the time behavior of the unobserved feeding has to be taken into account. It has been found to be realistic, with certain limitations, to assume a similar time behavior for the unobserved feeding as for the observed feeding (see, e.g., Ref. [4] and references therein). For the present study, this is justified as no structural effects dominate the feeding pattern to the levels of interest, i.e., the observed feeding transitions are not particularly slow. In fact, the effects arising from the unobserved feeding to the 2^+ and 4^+ states fall within the statistical uncertainties, which dominate the experimental errors of the final lifetimes. Further justification for this assumption can be found from the fact that the τ curves for all the states under investigation are constant, which should be the case when the feeding assumption is correct [21].

Lifetimes were extracted independently from the 134° and 158° data, the resulting lifetime being the average of these two values. Lifetimes of $\tau = 11.7(15)$ ps, 7.8(11) ps, and 2.9(12) ps were extracted for the 2^+, 4^+, and 6^+ states, respectively. An example of lifetime determination for the 2^+ state in ^{196}Po according to the principles of the DDCM is illustrated in Fig. 3.

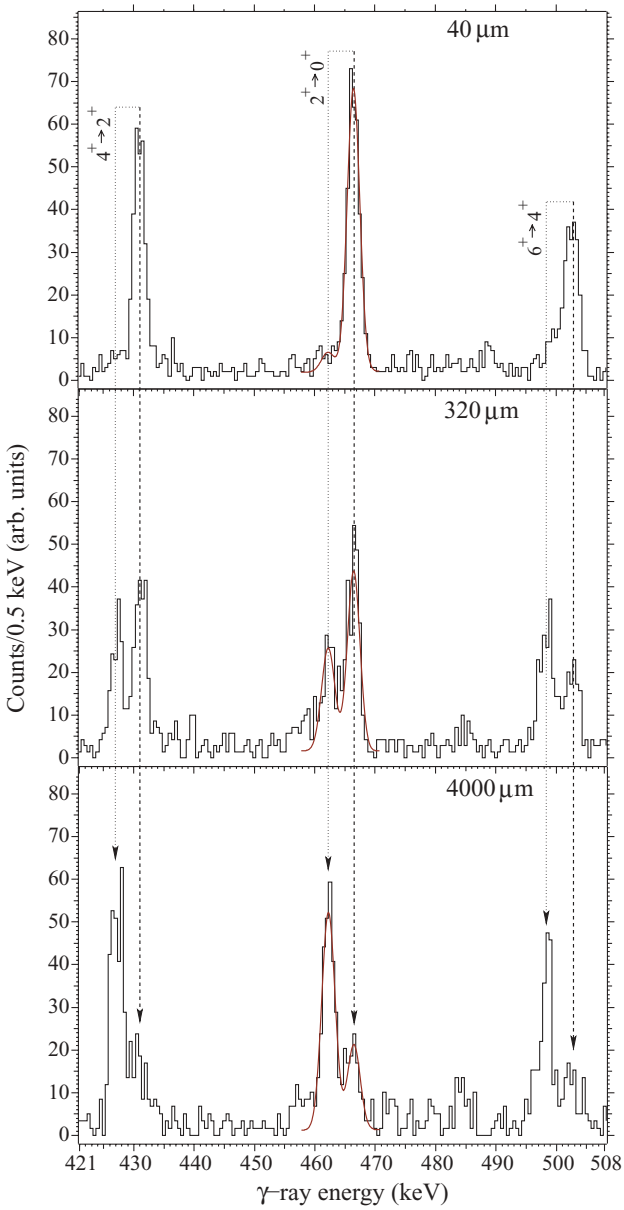

FIG. 2. (Color online) Singles RDT γ-ray spectra recorded at the three target-to-degrader distances (40 μm in the top panel, 320 μm in the middle panel, and 4000 μm in the bottom panel) with five JUROGAM detectors at 158°. Lines indicate the positions of the fully Doppler-shifted (dotted) and degraded (dashed) components of the transitions under investigation. For the $2^+ \rightarrow 0^+$ transition samples of typical two-component fits are also drawn.

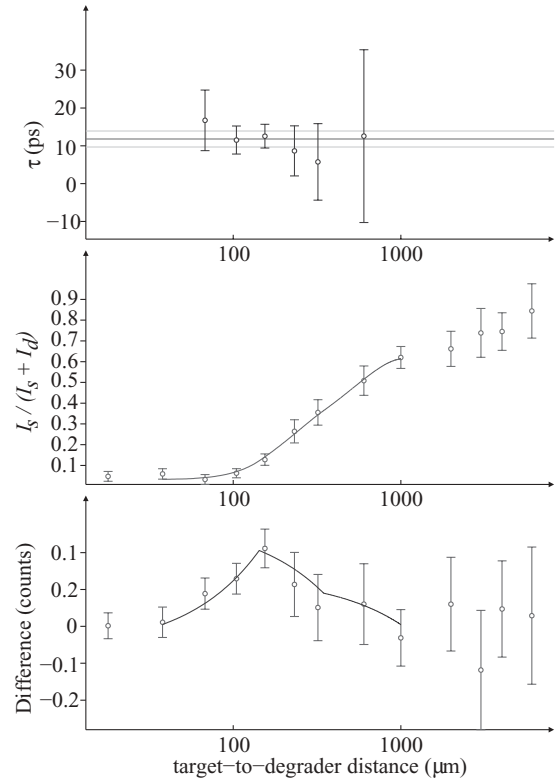

FIG. 3. Lifetime determination of the 2^+ yrast state in ^{196}Po. Lifetime values calculated for different distances are presented in the top panel along with the final lifetime value. The decay curve, recorded with five Ge detectors at 158° is shown in the middle panel. Only the relevant distances around the region of sensitivity [21] have been used for fitting. The bottom panel shows the difference of the quantities $I_s/(I_s + I_d)$ for the depopulating and direct feeding transitions. The line drawn through the experimental points is the derivative of the decay curve multiplied by the lifetime value.

III. DISCUSSION AND THEORETICAL DESCRIPTION

In the framework of the rotational model, where a rotating quadrupole deformed nucleus is assumed, absolute values for the transition quadrupole moment Q_t and the transition quadrupole deformation parameter $\beta_2^{(t)}$ can be assigned to the measured $B(E2)$ values [4]. Table I lists the values of the final lifetimes measured in the present study, along with the corresponding $|Q_t|$ and $|\beta_2^{(t)}|$ values.

On the other hand, taking the error bars into account, the trend of the measured $B(E2)$ values for the 2^+, 4^+, and 6^+

TABLE I. Electromagnetic properties of the low-lying yrast states in ^{196}Po. Transition energies E_γ are taken from Ref. [12]. Individual τ values extracted from the data recorded with Ge detectors at 158° and 134° (see text) are also given.

E_γ (keV)	I_i^π	$\tau_{158°}$ (ps)	$\tau_{134°}$ (ps)	τ_{final} (ps)	$B(E2)$ (W.u.)	$\lvert Q_t\rvert$ (eb)	$\lvert\beta_2^{(t)}\rvert$
463.1	2^+	11.8(20)	11.6(20)	11.7(15)	47(6)	4.0(3)	0.129(9)
427.9	4^+	7.4(20)	8.0(12)	7.8(11)	103(15)	4.9(4)	0.16(2)
499.1	6^+	3.0(16)	2.8(17)	2.9(12)	130(60)	5.3(11)	0.17(4)

yrast states could resemble that for a vibrator, falling between those expected for an ideal vibrator or rotor. However, if one were to exclude the intruder configurations in the description of the low-energy level structure of ^{196}Po, one would expect the collectivity of the yrast transitions to be significantly lower than what is observed. In Ref. [22] quasiparticle random phase approximation calculations have been carried out for ^{196}Po. In that theoretical framework the effect of particle-hole intruder structures cannot be taken into account. The calculated value of $B(E2; 2_1^+ \rightarrow 0^+) = 9.8$ W.u. obtained in Ref. [22] is considerably smaller than the experimental value of 47(6) W.u. measured in the present work. This supports the importance of the intruder structures in enhancing the collectivity of the yrast transitions in ^{196}Po.

The phonon model gives a schematic picture of the ^{196}Po spectrum which fails to explain the observed low-lying 0^+ state at 558 keV. In contrast, a shape coexistence picture can give a coherent view of the structure of ^{196}Po at low spin. It is also supported by other experimental data, such as level-energy systematics and the observed collectivity in neighboring nuclei.

The $|Q_t|$ values of Table I have been plotted in Fig. 4 with those for ^{194}Po and ^{186,188}Pb. The $|Q_t|$ value of the 2^+ state in ^{196}Po is slightly smaller than that of ^{194}Po. As expected on the basis of energy level systematics, deformed intruder structures lie higher in energy when moving away from the neutron midshell ($N = 104$) toward the shell closure at $N = 126$. The slight decrease of collectivity for the $2^+ \rightarrow 0^+$ transition in ^{196}Po compared to that in ^{194}Po is a sign of reduced intruder contribution in the ground state of ^{196}Po. However, the collectivity of the $2^+ \rightarrow 0^+$ transition in ^{196}Po is still rather high, compared to that of the corresponding transitions in ^{186,188}Pb, where dramatic differences in the structures of the ground states and the first 2^+ states have been observed. While in ^{194}Po similar structures for the ground state and the yrast 2^+ and 4^+ states are assumed [8], the smooth drop of $|Q_t|$ observed for the transitions in ^{196}Po suggests a smaller intruder contribution to the ground state than to the other yrast states of this nucleus.

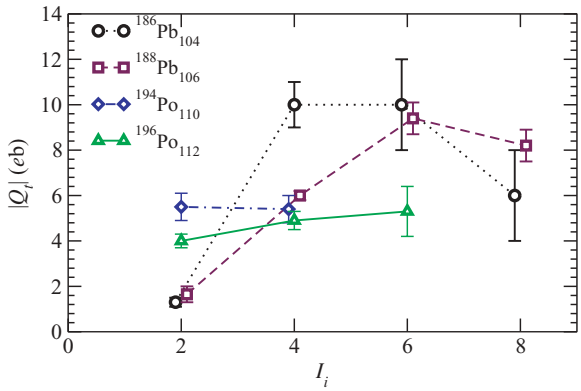

FIG. 4. (Color online) Transition quadrupole moments $|Q_t|$ taken from the present work and Ref. [8]. Some of the $|Q_t|$ values have been slightly offset from their actual I_i value to maintain the clarity of presentation.

To provide a comparison with the mixing amplitude of the ^{196}Po ground state deduced in Ref. [6], a rough estimate of this mixing can be extracted from the measured $B(E2)$ values using a simple two-band mixing scenario (similarly to that for the 2^+ state in ^{188}Pb [8]). It seems reasonable to assume that the yrast band is purely a quadrupole deformed band at a spin starting at $I^\pi = 4^+$. Assuming also that interband transitions are forbidden, one obtains a ground state wave function where the weight of the intruder configuration is dominant, being ~70%. This is in accordance with the trend of decreasing intruder contributions with increasing A derived from the observed level energies in Ref. [6] (*cf.* the oblate ground state in ^{194}Po [8]). However, the ~70% contribution of the deformed configuration to the ground state extracted in the present work is much higher than the ~10% of Ref. [6].

In contrast to the empirical two-band mixing model, the problem of mixing of spherical and deformed configurations in the lowest states of ^{196}Po has been studied theoretically using the same method as in Refs. [4,23]. This method is based on the configuration mixing of self-consistent mean-field wave functions with different intrinsic axial quadrupole moment projected on angular momentum. The Skyrme interaction SLy6 and a density-dependent pairing interaction have been used. An extensive description of the method can be found in Refs. [4,23]. Two key features of the model are that electromagnetic moments are directly obtained in the laboratory frame without the need for further assumptions and that its only parameters are contained in the effective interactions without any specific adjustment to nuclei around ^{196}Po.

The excitation energies obtained at the successive levels of the present method are plotted in Fig. 5 as a function of the axial intrinsic quadrupole moment, parametrized by a dimensionless parameter β_2. At the mean-field level, the deformation energy surface is extremely soft as a function of β_2, with several minima. After projection on angular momentum, deeper minima are obtained by the projection of oblate and prolate mean-field states. There are in fact two

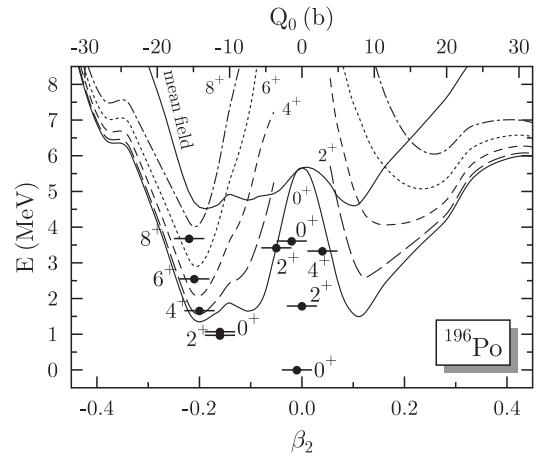

FIG. 5. Mean field and angular-momentum projected deformation energy curves as a function of the intrinsic deformation β_2 (bottom scale) and the the mass quadrupole moment (top scale) of the mean-field states. Selected collective states are plotted at their average intrinsic deformation (see text).

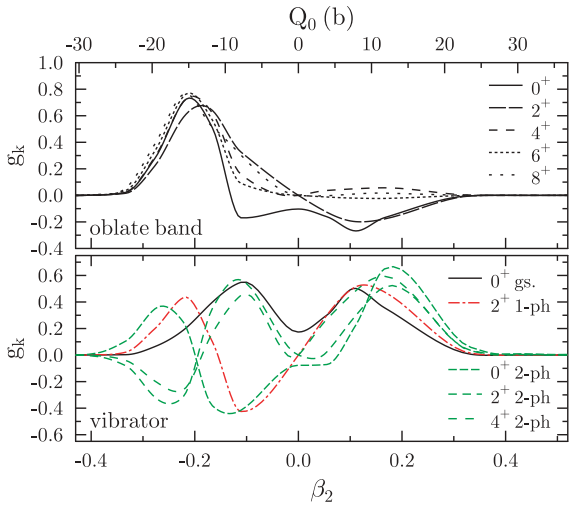

FIG. 6. (Color online) Collective wave functions g_k^J of the ground state and of the collective vibrational one-phonon (1-ph) and two-phonon (2-ph) states (the lower panel) and of the oblate states (upper panel) as a function of the intrinsic deformation β_2 of the mean-field states.

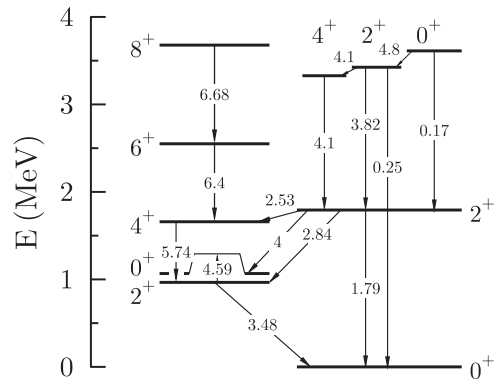

FIG. 7. Calculated level energies and Q_t values of the strongest transitions in ^{196}Po. The Q_t values are given in units of eb.

minima on the oblate side, the first at a very small deformation and the second, close in energy, at larger deformation. On the prolate side, there is only one minimum at a very small value of β_2. The final results are obtained after configuration mixing and are shown by dots positioned at an average deformation (see Refs. [4,23] for the definition of this mean value).

The corresponding collective wave functions g_k^J (see Refs. [4,23] for its definition and interpretation) are shown in Fig. 6. These figures suggest the separation of the low-lying spectrum into two coexisting structures. The first one is a spherical vibrational structure built on the ground state with a 2^+ one-phonon state at 1.79 MeV and a triplet of two-phonon states at 3.33 (4^+), 3.43 (2^+), and 3.61 (0^+) MeV. The second structure consists of an oblate band with its band head at an excitation energy around 1 MeV. One sees also in Fig. 6 that the collective wave functions of the second band are well localized at an intrinsic deformation β_2 around -0.22 while those of the first band are spread in the entire well, symmetrically around the spherical configuration. These two patterns are typical for rotational and vibrational bands. This result is rather similar to the one obtained for ^{194}Po in Ref. [8]. However, no prolate band is obtained for this heavier isotope, and the calculated spectrum is more spread.

Figure 6 indicates also that there is a mixing of both structures for several states. This is particularly obvious for the oblate 0^+ and 2^+ states, whose wave functions present a tail extending up to the prolate deformations. These mixings have an effect on the excitation energies: the 0^+ band head of the oblate band is pushed up by its mixing with the ground state, while the yrast oblate 2^+ state is pulled down by its mixing with the vibrational 2^+ state. As a result, the oblate band is strongly distorted at low spin, with the the 0^+ state lying at higher energy than the 2^+ state. This feature is consistent with data obtained from α-decay spectroscopy [6] where an excited 0^+ state slightly above the yrast 2^+ state has been observed (see Fig. 1).

Transition quadrupole moments Q_t resulting from the present calculations are shown in Fig. 7 for all the states in the spectrum. The Q_t values obtained for the oblate band ($I^\pi = 4^+$ and 6^+) and for the lowest 2^+ state (3.5, 5.7, and 6.3 eb, respectively) are in reasonable agreement with the experimental data [cf. respective values of 4.0(3), 4.9(4) and 5.3(11) eb]. They increase along the band, showing that, as expected, the mixing between the oblate and the vibrational configurations decreases with increasing spin. However, the Q_t value obtained for the $2^+ \rightarrow 0^+$ transition is only $\sim$10% lower than that in ^{194}Po, compared with the experimentally observed $\sim$30% decrease, suggesting a larger degree of mixing for the ground state of ^{196}Po than that of ^{194}Po. The fact that the experimental Q_t values are close to those calculated for the oblate structure and significantly higher than the calculated Q_t values for the vibrational structure, further supports the assumption of predominantly intruder yrast states in ^{196}Po.

The calculated quadrupole moments between the states which have been identified to form the vibrational band have a pattern which supports this interpretation. The theoretical Q_t values obtained for the transitions between the two-phonon states and the one-phonon 2^+ state are significantly higher than that for the following transition to the ground state. However, for an unknown reason, the Q_t value for the transition from the third 0^+ state is low compared to the corresponding values from the other two-phonon states. The collectivity of the transitions between the multiphonon states in the present work is generally lower than that for the transitions within the oblate band, as expected for a vibrational structure.

The picture that emerges from the present calculation is different from the interpretation made in Ref. [12], where the whole low-energy level scheme is associated with the simple vibrator. The method that has been used in the present work overestimates excitation energies. This deficiency of the model is common to the two other variants of the configuration mixing method, which are based either on a finite range interaction [24] or on a relativistic mean-field Lagrangian [25]. As shown using schematic interactions [26], it is probably related to the time-reversal symmetry imposed to the mean field and should be cured by the projection of mean-field wave functions constructed with a cranking constraint. This would drastically increase the computing time and is not feasible with

the present computer facilities. However, numerous applications have shown that geometrical properties, in particular transition probabilities, are satisfactorily described (see for instance Refs. [3,4,23,27]). The theoretical framework used in the present work incorporates the intruder configurations and describes the experimental data in a coherent manner, including the low-lying 0^+ state, which was not the case in Ref. [12].

IV. SUMMARY AND CONCLUSIONS

To conclude, the lifetimes of the low-lying yrast states in ^{196}Po have been measured by utilizing the RDDS technique. The $|Q_t|$ values extracted from the measured lifetimes suggest the 2^+ and 4^+ states being predominantly intruder character while the drop of the $|Q_t|$ value for the $2^+ \rightarrow 0^+$ transition compared to higher lying transitions suggests the mixing of the spherical and oblate structures in the ground state of ^{196}Po. A reduced collectivity was observed compared to earlier measurements in ^{194}Po, consistent with the picture of increasing excitation energy of the intruder configurations when going away from the neutron midshell at $N = 104$ toward $N = 126$. The present calculations exploiting configuration mixing of angular momentum projected mean-field states indicate the mixing of the vibrational and rotational configurations at low spin, in agreement with the experimental data.

ACKNOWLEDGMENTS

This work has been supported through EURONS (European Commission contract no. RII3-CT-2004-506065), the Academy of Finland under the Finnish Centre of Excellence Programme 2006–2011 (Nuclear and Accelerator Based Physics contract 213503), the UK STFC, and by the PAI-P5-07 of the Belgian Office for Scientific Policy. The UK/France (STFC/IN2P3) Loan Pool and GAMMAPOOL network are acknowledged for the EUROGAM detectors of JUROGAM. C.S. acknowledges the support of the Academy of Finland, Contract No. 209430.

[1] J. L. Wood, K. Heyde, W. Nazarewicz, M. Huyse, and P. Van Duppen, Phys. Rep. **215**, 101 (1992).
[2] R. Julin, K. Helariutta, and M. Muikku, J. Phys. G **27**, R109 (2001).
[3] J. Pakarinen *et al.*, Phys. Rev. C **75**, 014302 (2007).
[4] T. Grahn *et al.*, Nucl. Phys. **A801**, 83 (2008).
[5] P. Van Duppen, E. Coenen, K. Deneffe, M. Huyse, K. Heyde, and P. Van Isacker, Phys. Rev. Lett. **52**, 1974 (1984).
[6] N. Bijnens, P. Decrock, S. Franchoo, M. Gaelens, M. Huyse, H.-Y. Hwang, I. Reusen, J. Szerypo, J. von Schwarzenberg, J. Wauters, J. G. Correia, A. Jokinen, and P. Van Duppen (ISOLDE Collaboration), Phys. Rev. Lett. **75**, 4571 (1995).
[7] F. R. May, V. V. Paskevich, and S. Frauendorf, Phys. Lett. **B68**, 113 (1977).
[8] T. Grahn *et al.*, Phys. Rev. Lett. **97**, 062501 (2006).
[9] A. N. Andreyev *et al.*, Phys. Rev. Lett. **82**, 1819 (1999).
[10] D. R. Wiseman *et al.*, Eur. Phys. J. A **34**, 275 (2007).
[11] K. Van de Vel *et al.*, Phys. Rev. C **68**, 054311 (2003).
[12] L. A. Bernstein *et al.*, Phys. Rev. C **52**, 621 (1995).
[13] A. M. Oros, K. Heyde, C. De Coster, B. Decroix, R. Wyss, B. R. Barrett, and P. Navratil, Nucl. Phys. **A645**, 107 (1999).
[14] D. Alber *et al.*, Z. Phys. A **339**, 225 (1991).
[15] M. Leino *et al.*, Nucl. Instrum. Methods B **99**, 653 (1995).
[16] C. W. Beausang *et al.*, Nucl. Instrum. Methods A **313**, 37 (1992).
[17] R. D. Page *et al.*, Nucl. Instrum. Methods B **204**, 634 (2003).
[18] E. S. Paul *et al.*, Phys. Rev. C **51**, 78 (1995).
[19] I. H. Lazarus *et al.*, IEEE Trans. Nucl. Sci. **48**, 567 (2001).
[20] P. Rahkila, Nucl. Instrum. Methods A **595**, 637 (2008).
[21] A. Dewald, S. Harissopulos, and P. von Brentano, Z. Phys. A **334**, 163 (1989).
[22] W. Younes and J. A. Cizewski, Phys. Rev. C **55**, 1218 (1997).
[23] M. Bender, P. Bonche, T. Duguet, and P.-H. Heenen, Phys. Rev. C **69**, 064303 (2004).
[24] T. R. Rodríguez, J. L. Egido, and A. Jungclaus, Phys. Lett. **B668**, 410 (2008).
[25] T. Nikšić, D. Vretenar, G. A. Lalazissis, and P. Ring, Phys. Rev. Lett. **99**, 092502 (2007).
[26] D. Baye and P.-H. Heenen, Phys. Rev. C **29**, 1056 (1984).
[27] T. Duguet, M. Bender, P. Bonche, and P.-H. Heenen, Phys. Lett. **B559**, 201 (2003).